JOURNAL OF APPLIED CRYSTALLOGRAPHY

Volume 53 (2020)

Supporting information for article:

Accurate high-resolution single-crystal diffraction data from a Pilatus3 X CdTe detector

Lennard Krause, Kasper Tolborg, Thomas Bjørn Egede Grønbech, Kunihisa Sugimoto, Bo Brummerstedt Iversen and Jacob Overgaard

S1. FeSb2 Att vs Exp (ddm) at fixed attenuation

See attached pdf file kc5106sup4.pdf

S2. FeSb2 Att vs Att (ddm) at fixed exposure time

See attached pdf file kc5106sup5.pdf

S3. Detector pixel-by-pixel comparison

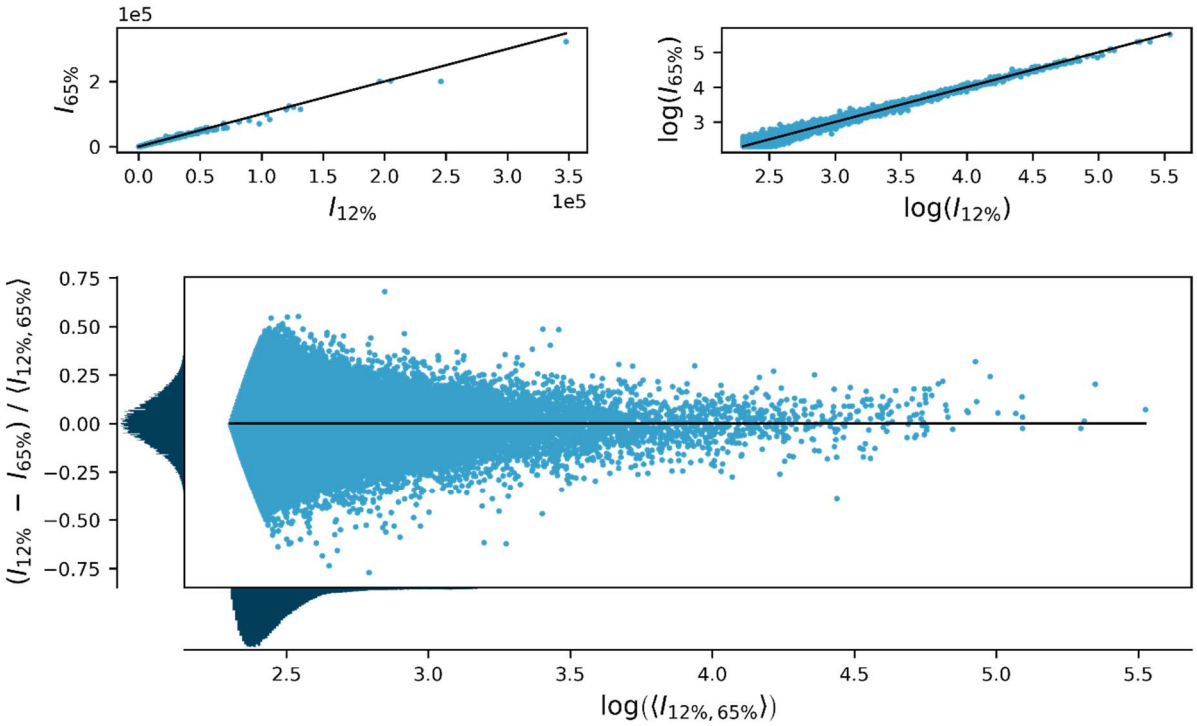

Figure S1 Pixel-by-pixel comparison of the combined frames of the first run (360 images) of the data collected with 12% and 65% of the maximum beam flux. The data was scaled (scale factor of 4.274) and a low intensity cutoff was applied at 200 counts.

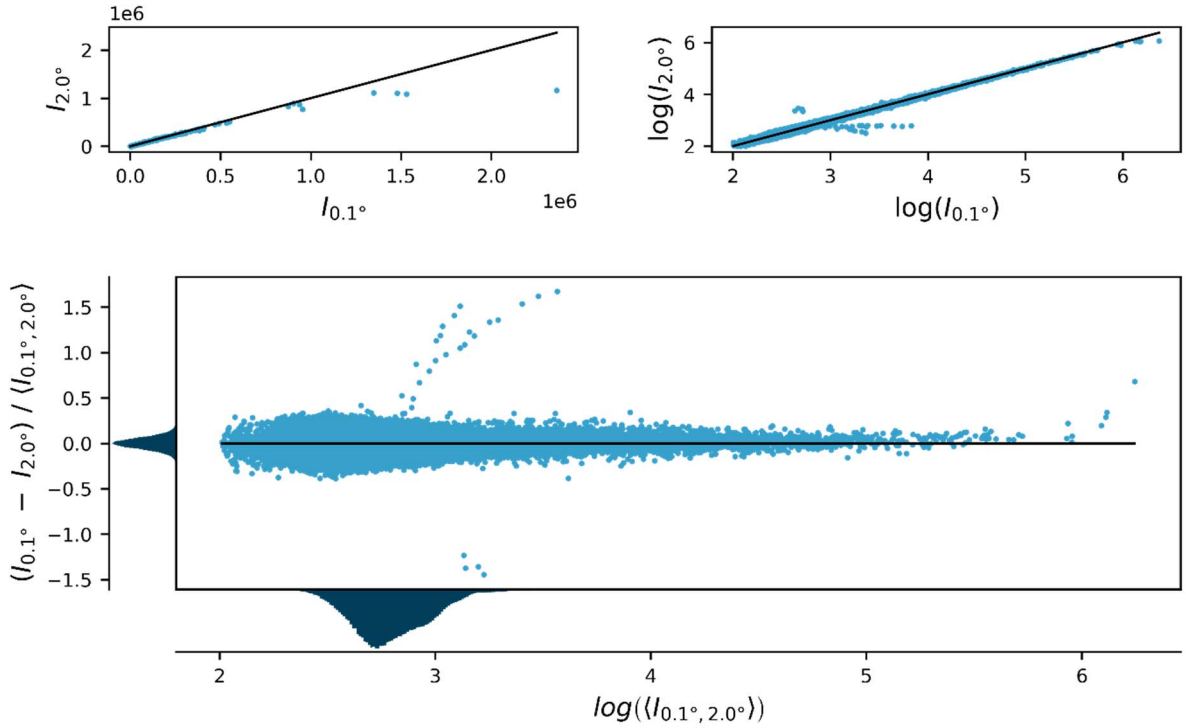

Figure S2 Plot showing the unprocessed pixel-by-pixel comparison of frames acquired from different slicing experiments and hereby a direct, unprocessed pixel-by-pixel comparison. The individual frames of two slicing experiments (0.1°, 900 images; 2.0°, 45 images) are combined to give two images with the same accumulated exposure time and scan width. The plot shows the same trend for the strong data and no indication of any other bias.

S4. Effect of beam flux, extinction and exposure time on the electron density model

Beam flux [%]#	Exposure [s]	GoF	Data	Extinction	R(F^2)	e_{gross}
12	0.2	0.9069	2469	11.5	0.0232	28.2598
12	0.2	0.9419	2469	None	0.0272	30.4041
12	0.5	0.9577	2491	7.8	0.0181	21.6559
12	0.5	0.9747	2491	None	0.0206	23.4621
12	1.0	0.9657	2497	8.1	0.0151	16.6616
12	1.0	0.9896	2497	None	0.0176	18.5596
12	2.0	0.9911	2502	7.6	0.0151	16.0055
12	2.0	1.0087	2502	None	0.0176	18.1266
12	4.0	1.0062	2504	8.8	0.0148	15.0408
12	4.0	1.0317	2504	None	0.0171	18.1257
31	0.2	0.9305	2476	13.1	0.0206	24.3815
31	0.2	0.9839	2476	None	0.0256	27.1
31	0.5	0.9239	2503	11.6	0.0167	18.2965
31	0.5	0.9660	2503	None	0.0209	22.1119
31	1.0	0.9592	2493	10.3	0.0153	16.0508
31	1.0	0.9940	2493	None	0.0187	19.9466
31	2.0	0.9962	2504	12	0.0145	15.1029
31	2.0	1.0445	2504	None	0.0192	20.1886
31	4.0	1.0192	2510	10.8	0.014	14.626
31	4.0	1.0567	2510	None	0.018	19.6108
65	0.2	0.9392	2499	21.7	0.0163	18.5911
65	0.2	1.1275	2499	None	0.0267	28.4948
65	0.5	0.9783	2501	20.4	0.0148	15.714
65	0.5	1.1587	2501	None	0.0247	26.5884
65	1.0	1.0003	2504	20.6	0.0145	15.0017
65	1.0	1.1684	2504	None	0.0243	27.1425
65	2.0	1.0332	2508	21.7	0.0137	14.1569
65	2.0	1.2321	2508	None	0.0246	26.4792
100	0.2	0.9621	2502	26.3	0.0144	15.9226
100	0.2	1.3000	2502	None	0.0288	30.6525
100	0.5	1.0041	2509	28.9	0.0126	13.4989
100	0.5	1.4388	2509	None	0.0304	32.0323
100	1.0	1.0304	2506	30.7	0.0132	14.1031
100	1.0	1.5559	2506	None	0.0315	36.8259

#: In percent of the maximum beam flux.

S5. Effect of attenuation on the intensities

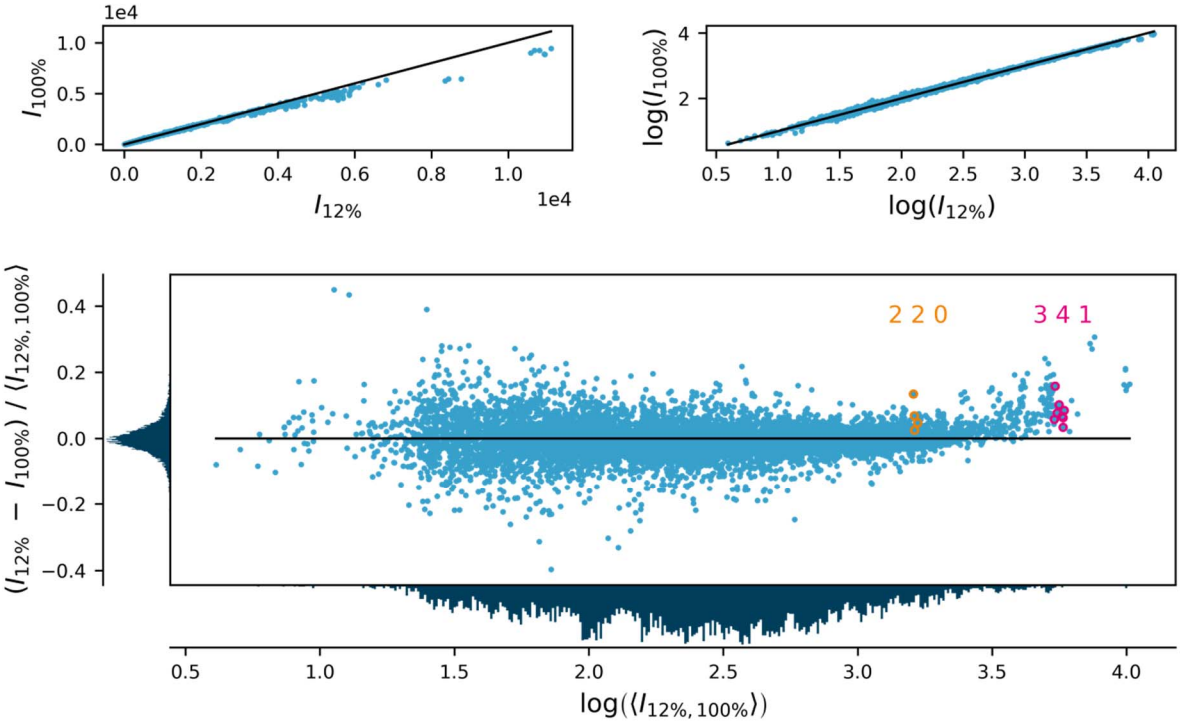

Figure S3 Comparison of integrated, scaled and averaged diffraction intensities of $FeSb_2$ collected with 12 % and 100 % of the full beam intensity with the reflections 3 4 1 and 2 2 0 (plus their equivalents) highlighted.

S6. SAINT: Spot profile fitting

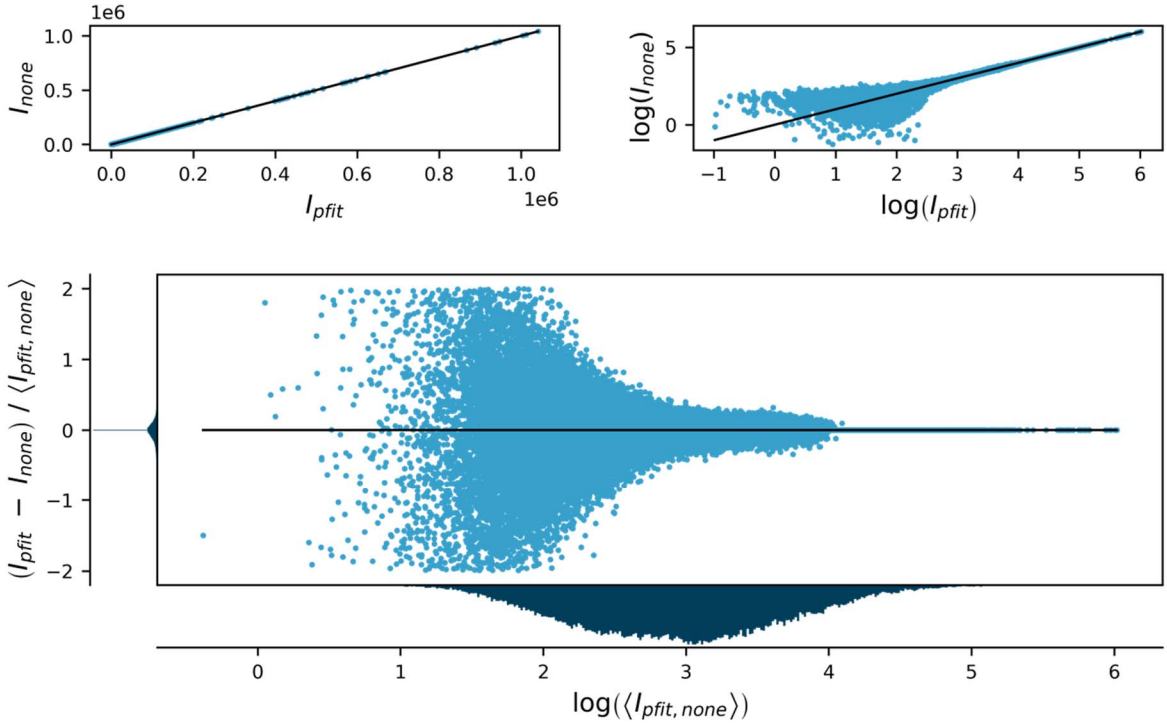

Figure S4 Supplement for Figure 7, intensity comparison of data integrated using LS-fitting (pfit) and without (none), without an I/σ cutoff.

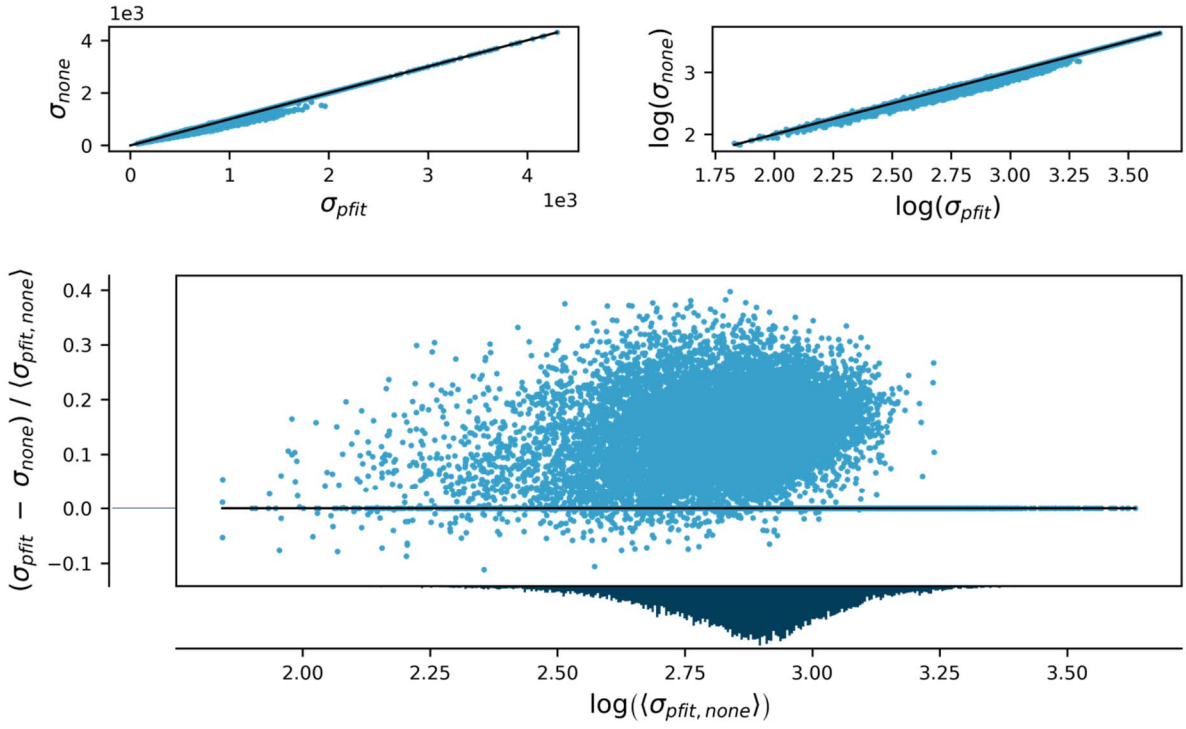

Figure S5 Comparison similar to Figure 7, however, with an I/σ cutoff of 3.0 applied.

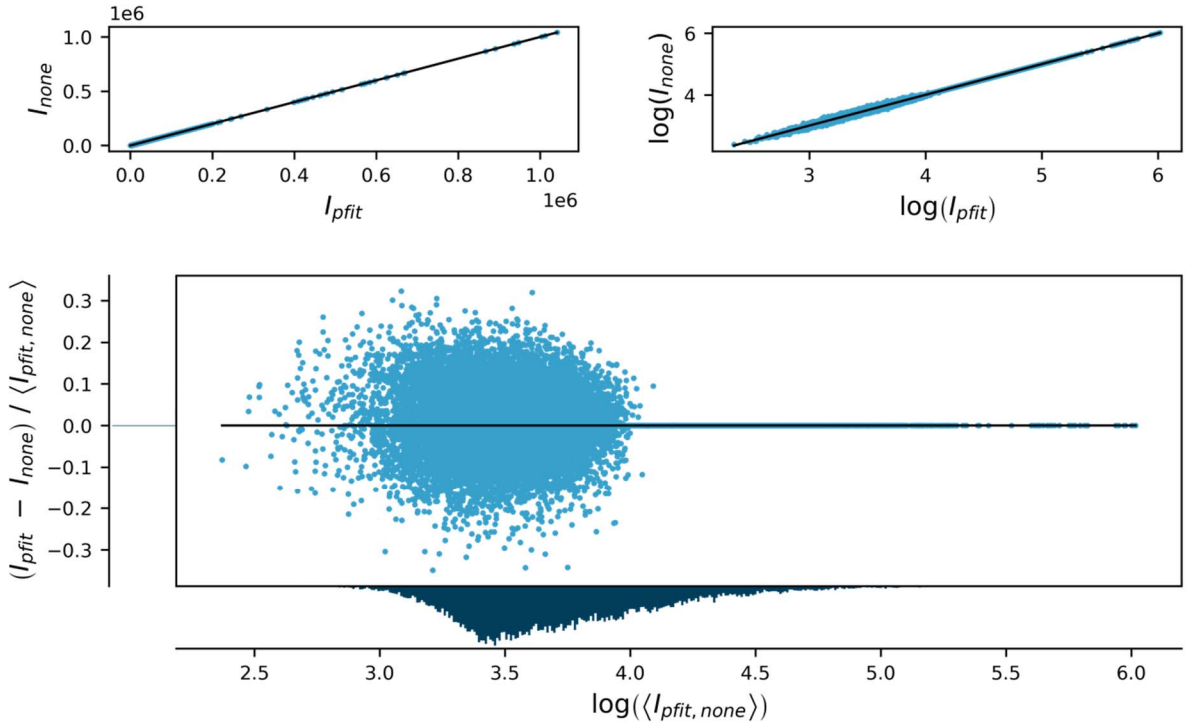

Figure S6 Comparison similar to Figure S4, however, with an I/σ cutoff of 3.0 applied.

S7. SAINT: Best-plane background and recurrence method

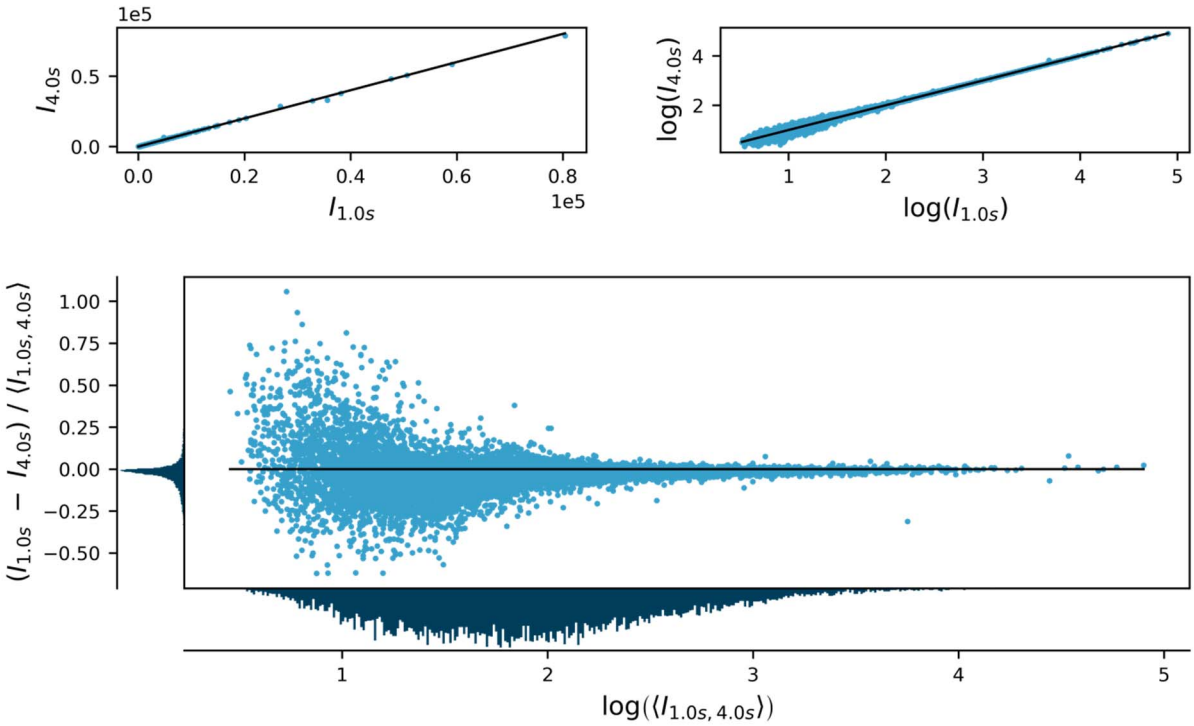

Figure S7 Best-plane background estimation compared for two exposure times (1.0 s and 4.0 s)

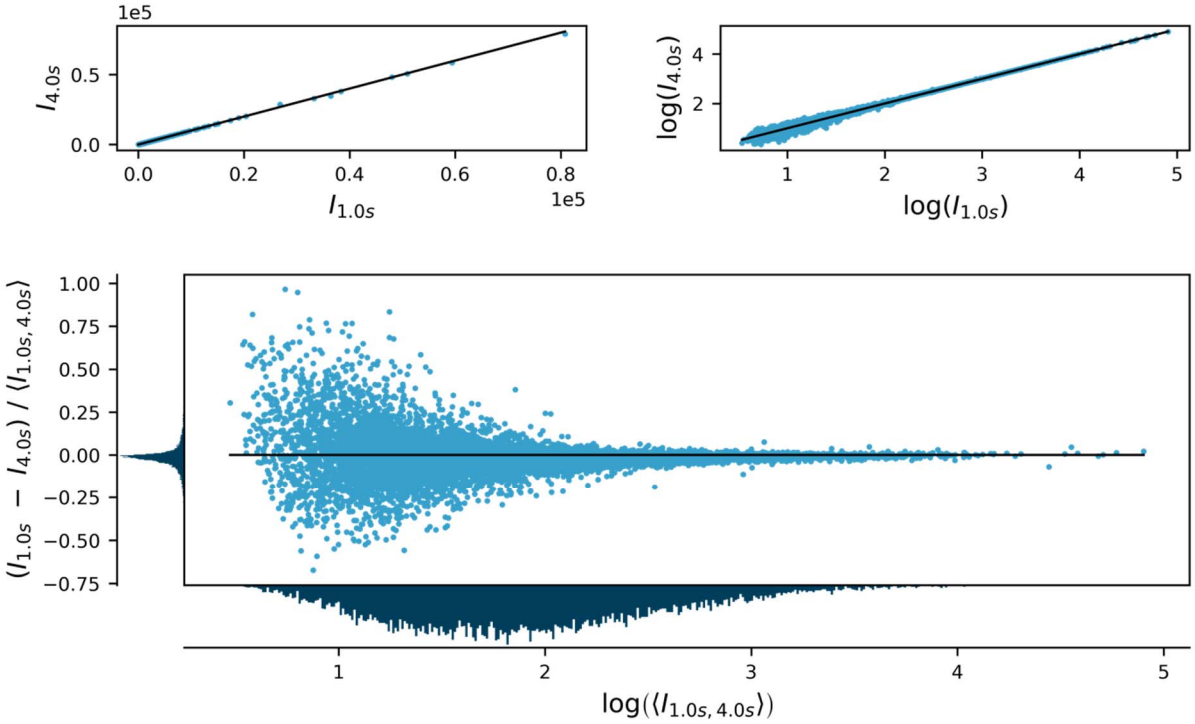

Figure S8 Recurrence background estimation compared for two exposure times (1.0 s and 4.0 s)

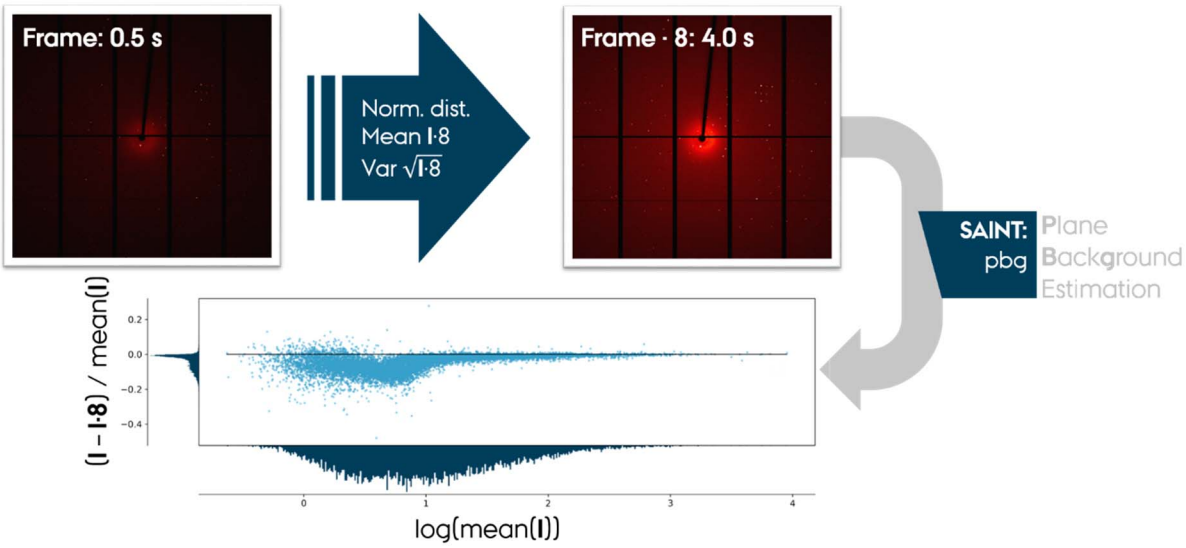

Figure S9 To exclude systematics in the data being responsible for the differences we constructed artificial data to simulate a perfect photon-counting detector, a program was written to manipulate images accordingly. The algorithm generates new images pixel by pixel, calculating a new pixel value c_i using a normal distribution around the value $c_i * m$ and a spread sqrt($c_i * m$) assuming Poisson noise. Two images were generated, one with the original intensities (but now more noisy) and a second with manipulated intensities, that were to be compared. The rationale behind the addition of Poisson noise was that a simple pixel-by-pixel multiplication resulted in ragged images with unphysical intensity distributions in the low-count areas, significantly affecting the background estimation of the integration routine.

S8. SADABS/SORTAV comparison: Exposure times

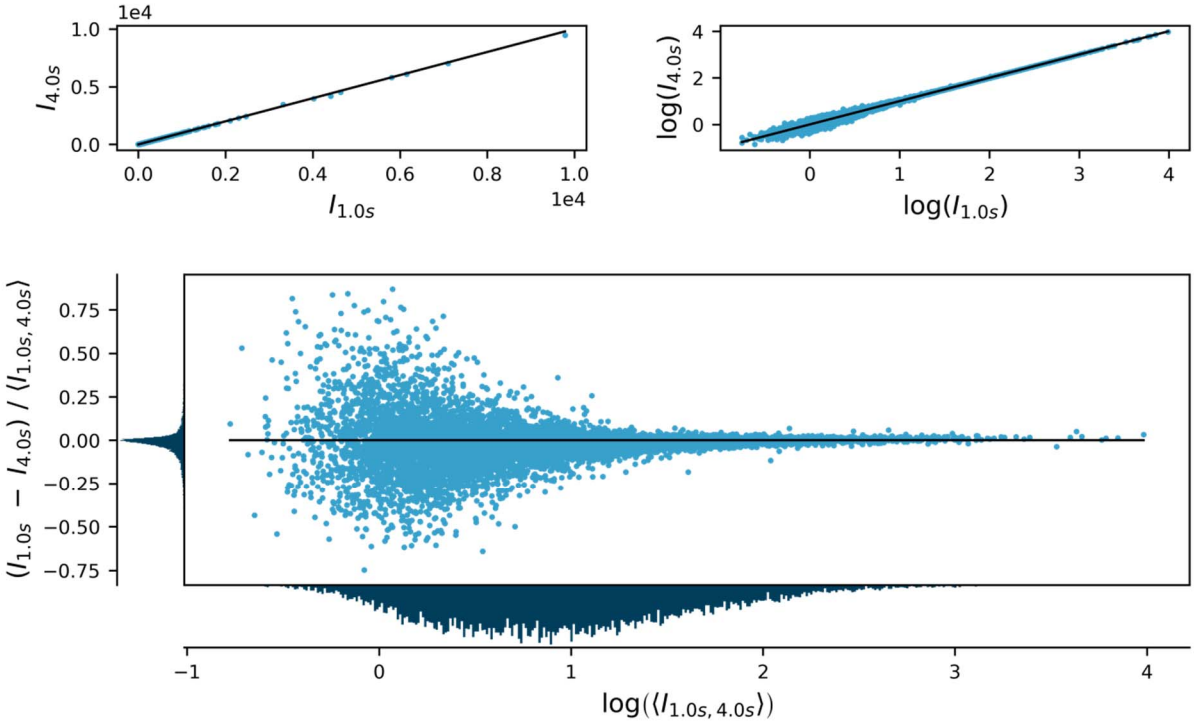

Figure S10 SADABS averaged equivalents compared for two exposure times (1.0 s and 4.0 s)

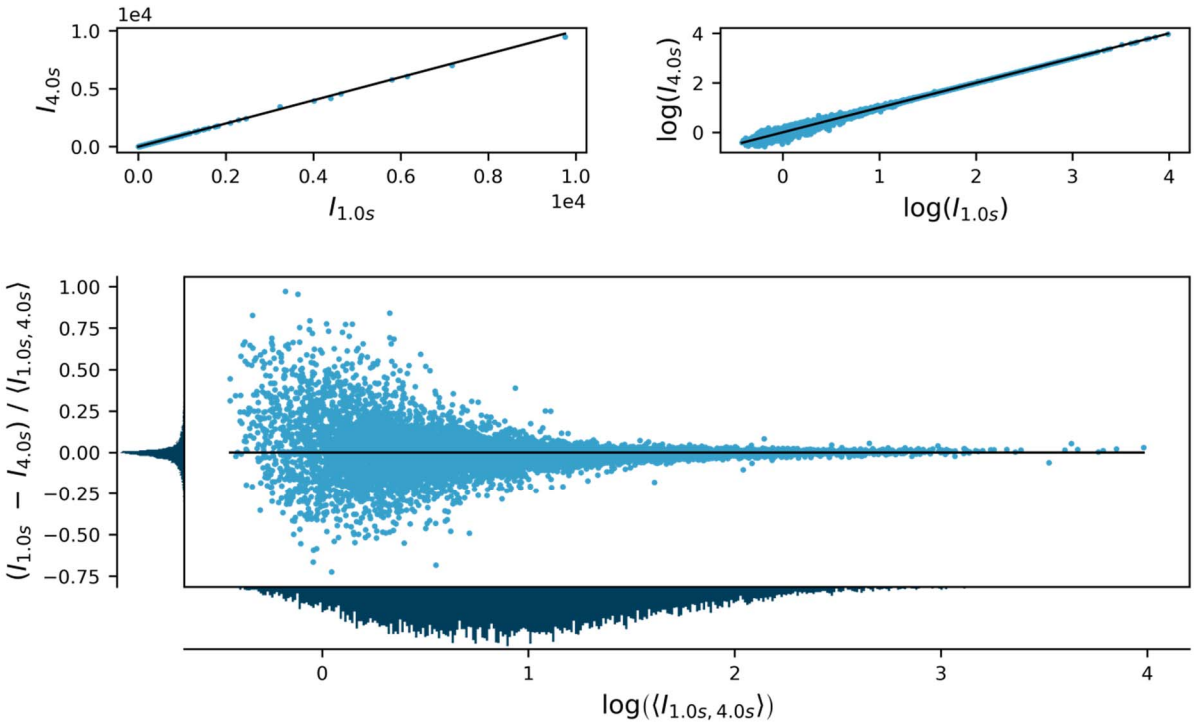

Figure S11 SORTAV averaged equivalents compared for two exposure times (1.0 s and 4.0 s)

S9. Skewness of the distribution of equivalent reflections

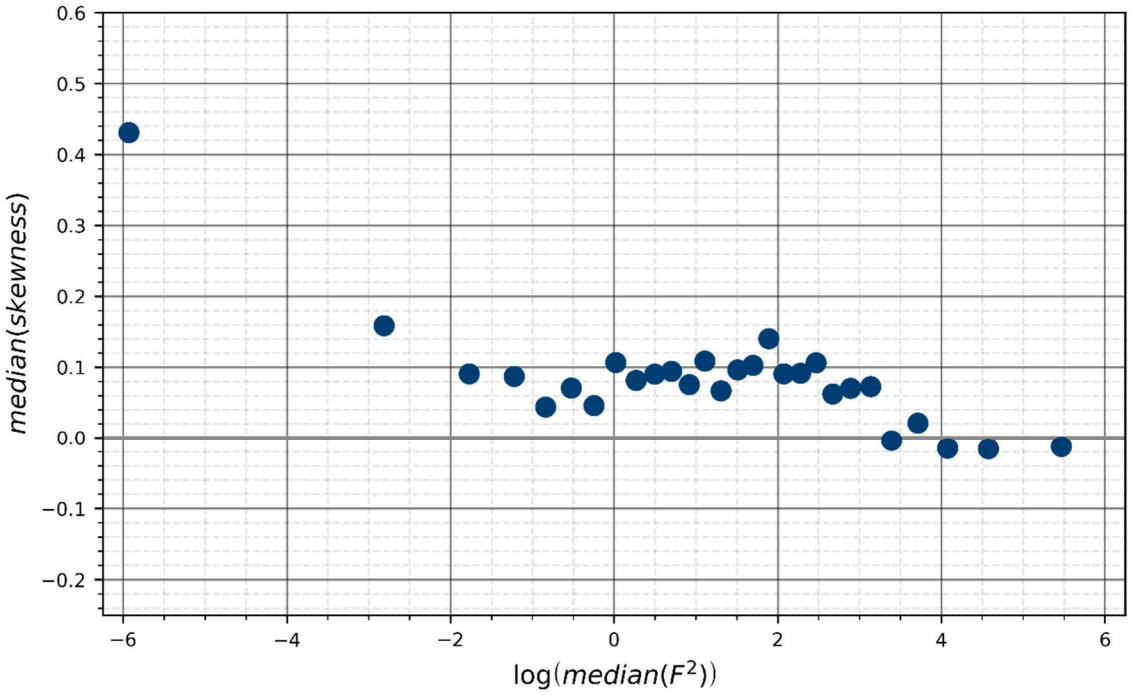

Figure S12 Skewness of the distribution of equivalent reflections versus the median intensity for unmerged data (binned) collected with an exposure time of 0.5 s.

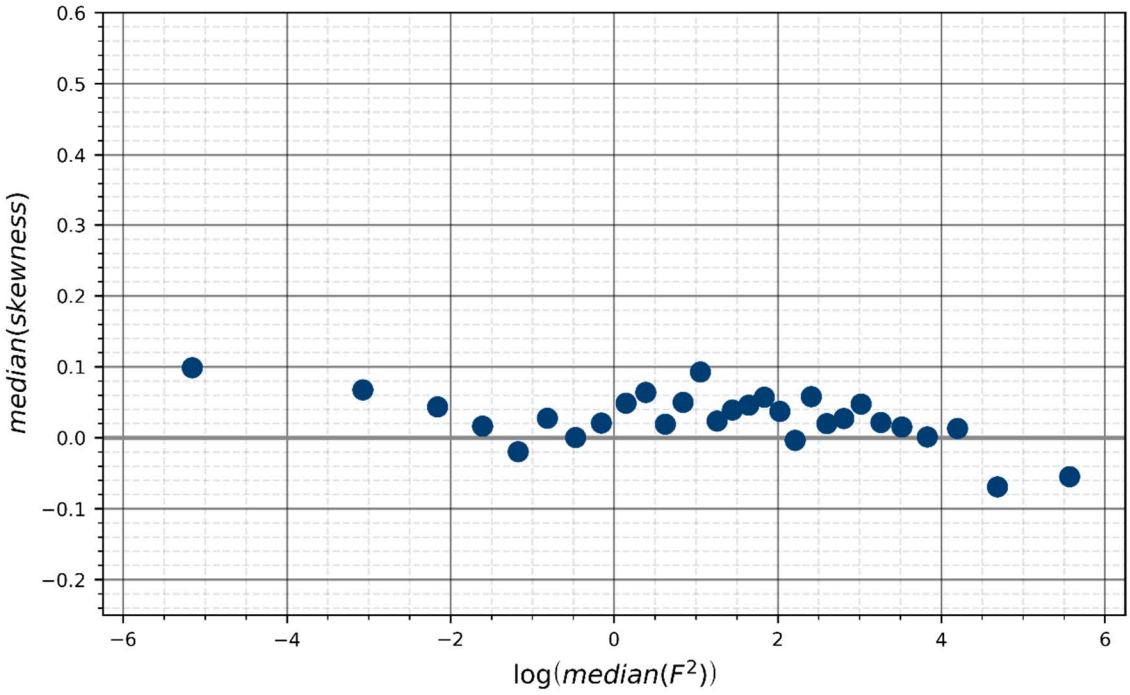

Figure S13 Skewness of the distribution of equivalent reflections versus the median intensity for unmerged data (binned) collected with an exposure time of 4.0 s.

S10. Systematic bias for weak data in data averaging

Artificial data was generated from a structure-factor file (*fco*) in combination with its unprocessed intensity file (*raw*, obtained directly from the integration software SAINT). The intensities in the *fco* were used as the expectation values to generate new intensities $I_{hkl,i}$ (integers, number of photons) following a random Poisson distribution and the number of generated values (i) matched the multiplicity of equivalent reflections in the *raw* file. The error $\sigma(I_{hkl,i})$ of the new intensities was chosen to reflect only Poisson noise ($\sqrt{I}$) with a lower boundary of 1. The calculated artificial $I_{hkl,i}$ and $\sigma(I_{hkl,i})$ were then used to replace the values in the *raw* file. This artificial *raw* file was processed using SADABS producing an unmerged *hkl* file with a suppressed error model (K = 1.0, g = 0.0) and an averaged *hkl* file (using error model 5, the values obtained for K ranged from 0.997 to 1.008 and g refined to 0.0028). The unmerged *hkl* was subsequently averaged using SORTAV. The following two plots show the difference between the ideal data (I_{fco}) and the averaged data (I_{sad}, I_{sor}). Deviations are only visible in the weak intensity region; however, systematic errors are only visible for the SADABS averaged data.

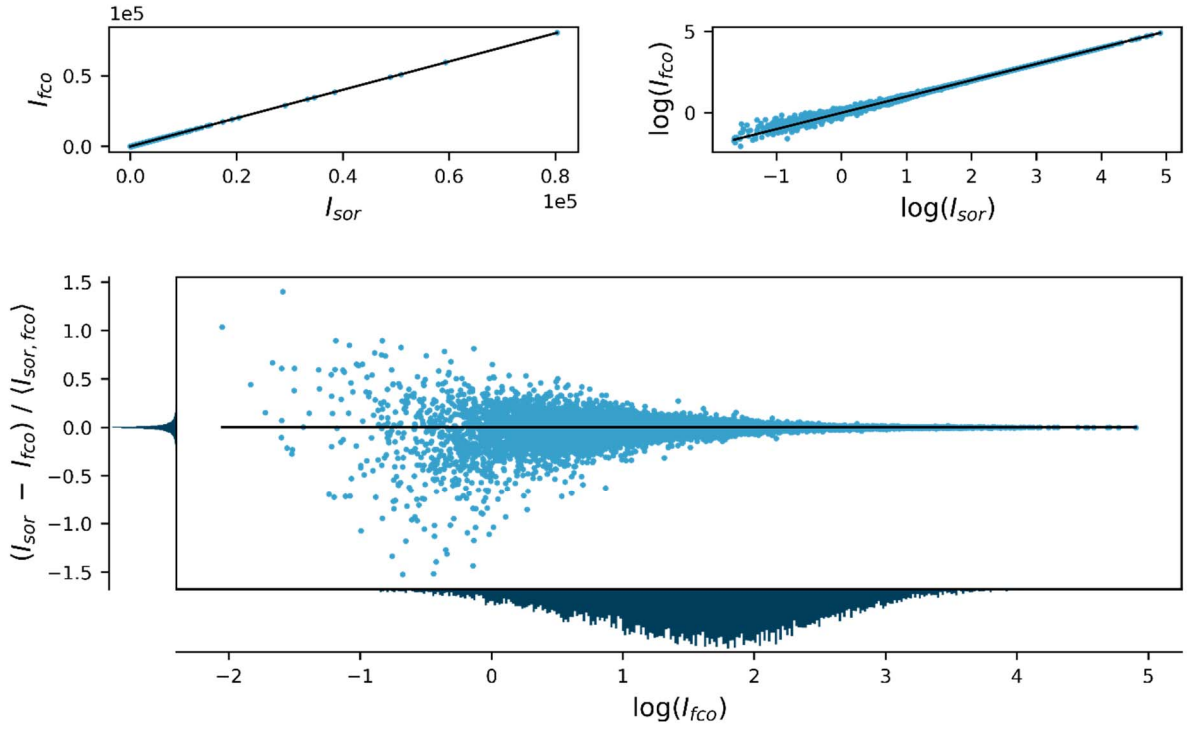

Figure S14 Averaging performance of SORTAV, comparison of the averaged intensities (I_{sor}) and the ideal data (I_{fco}).

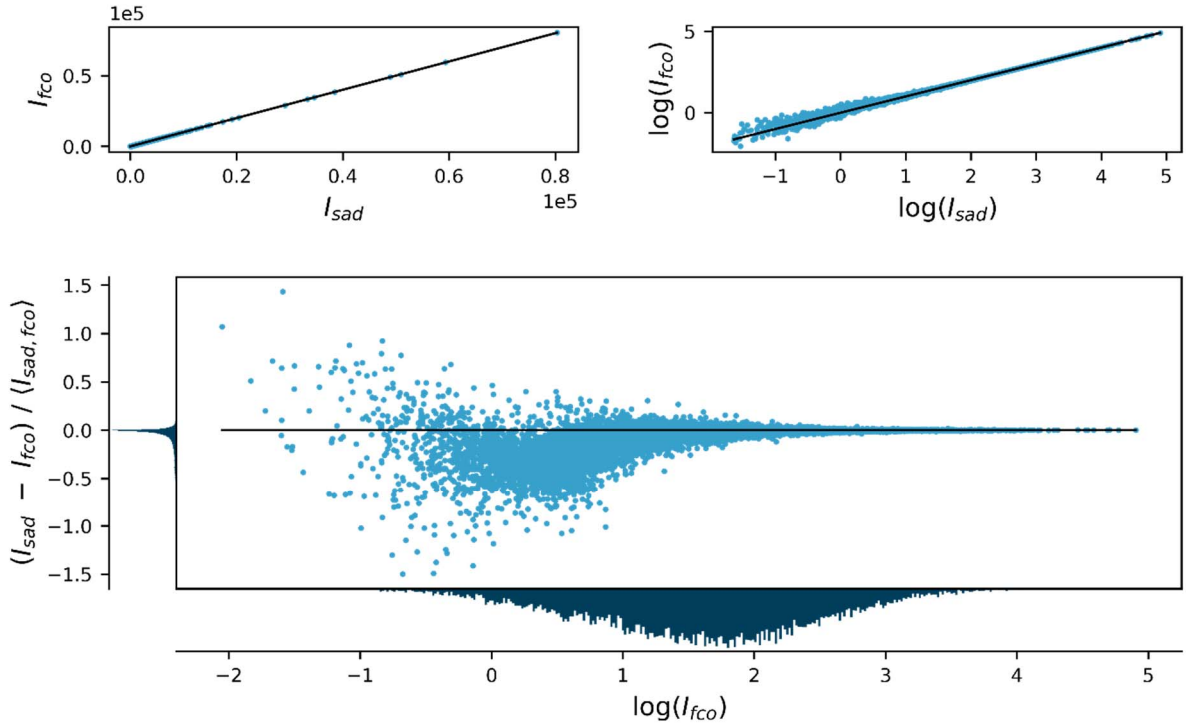

Figure S15 Averaging performance of SADABS, comparison of the averaged intensities (I_{sad}) and the ideal data (I_{fco}).

S11. SADABS/SORTAV comparison: Normal probability and scale factor plots for Rubrene

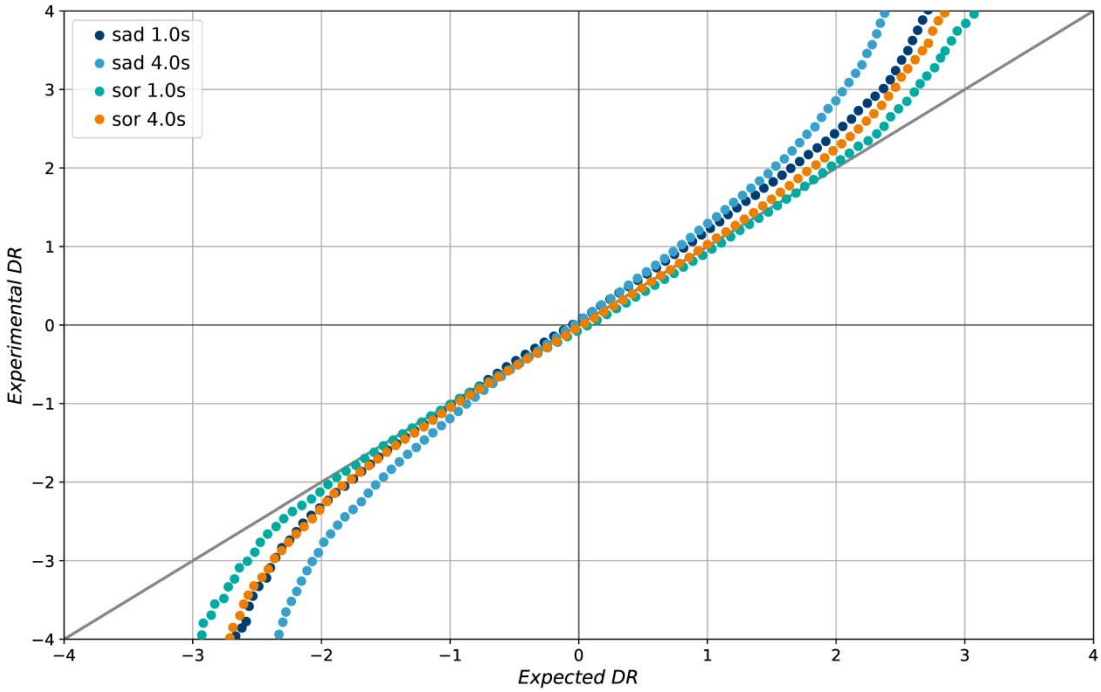

Figure S16 Normal-probability plot for models derived from either SADABS (sad) or SORTAV (sor) and two exposure times (1.0s, 4.0s)

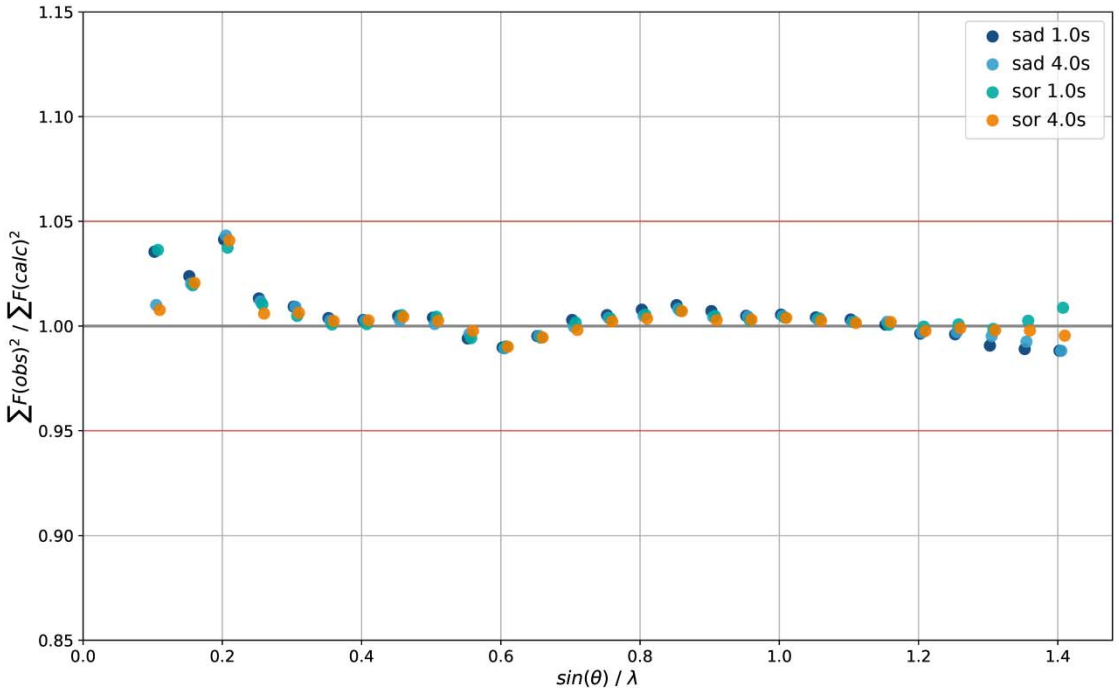

Figure S17 Scale-factor plot for models derived from either SADABS (sad) or SORTAV (sor) and two exposure times (1.0s, 4.0s)

S12. IP/P3 comparison: Rubrene

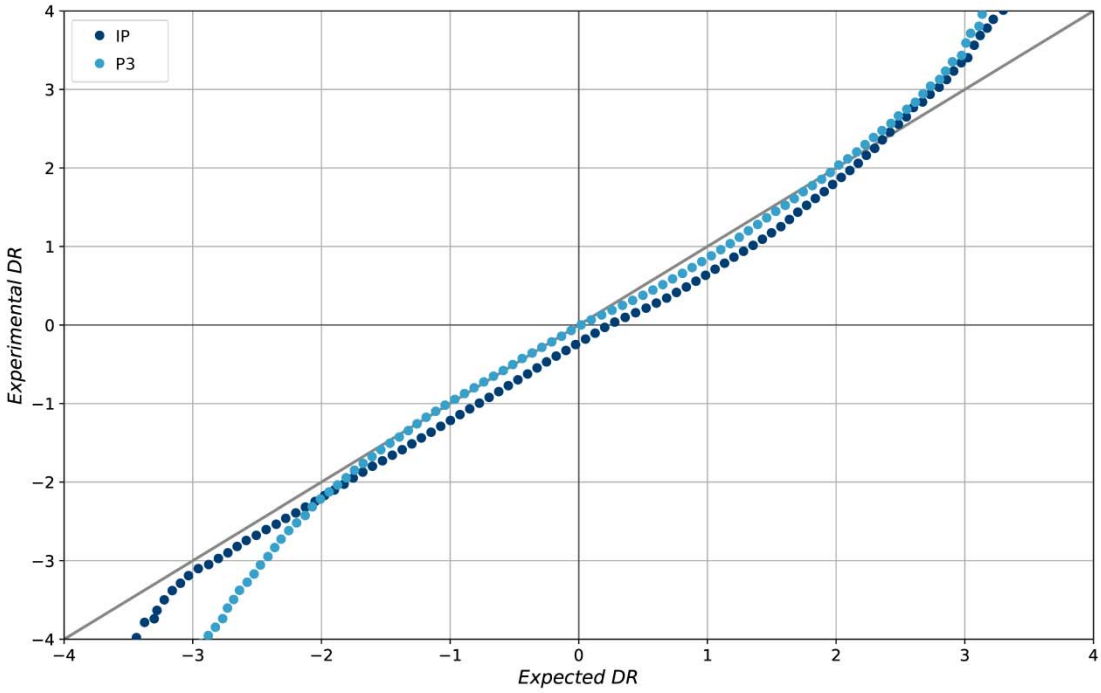

Figure S18 Normal-probability plot for models derived from image plate (IP) and Pilatus3 (P3) data.

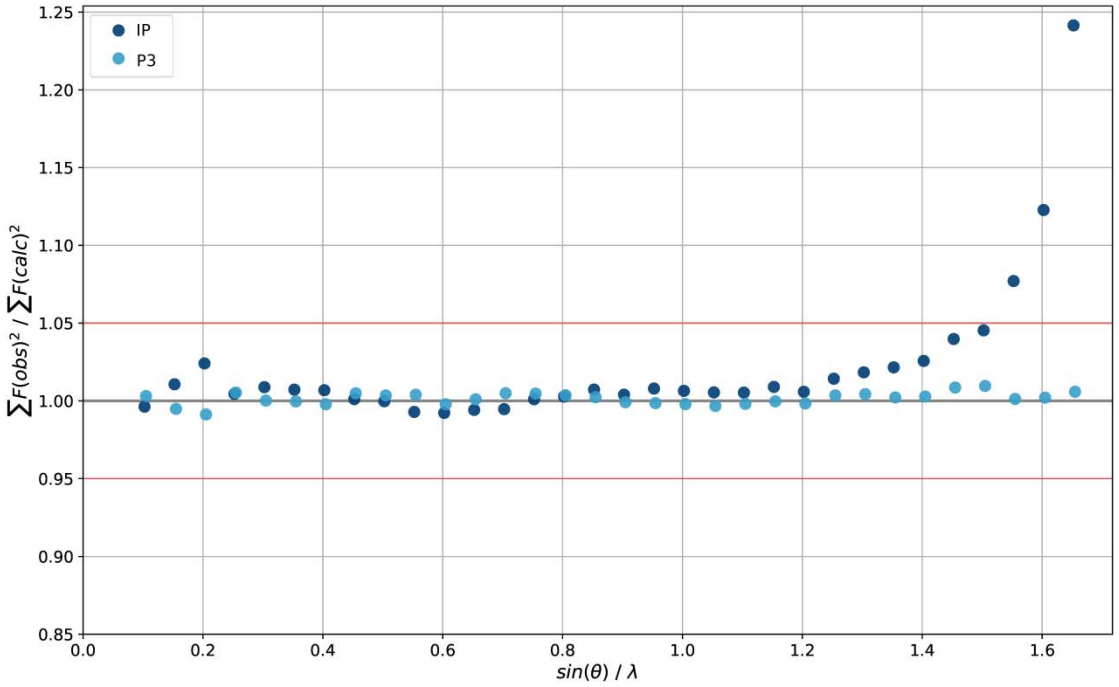

Figure S19 Scale-factor plot for models derived from image plate (IP) and Pilatus3 (P3) data.

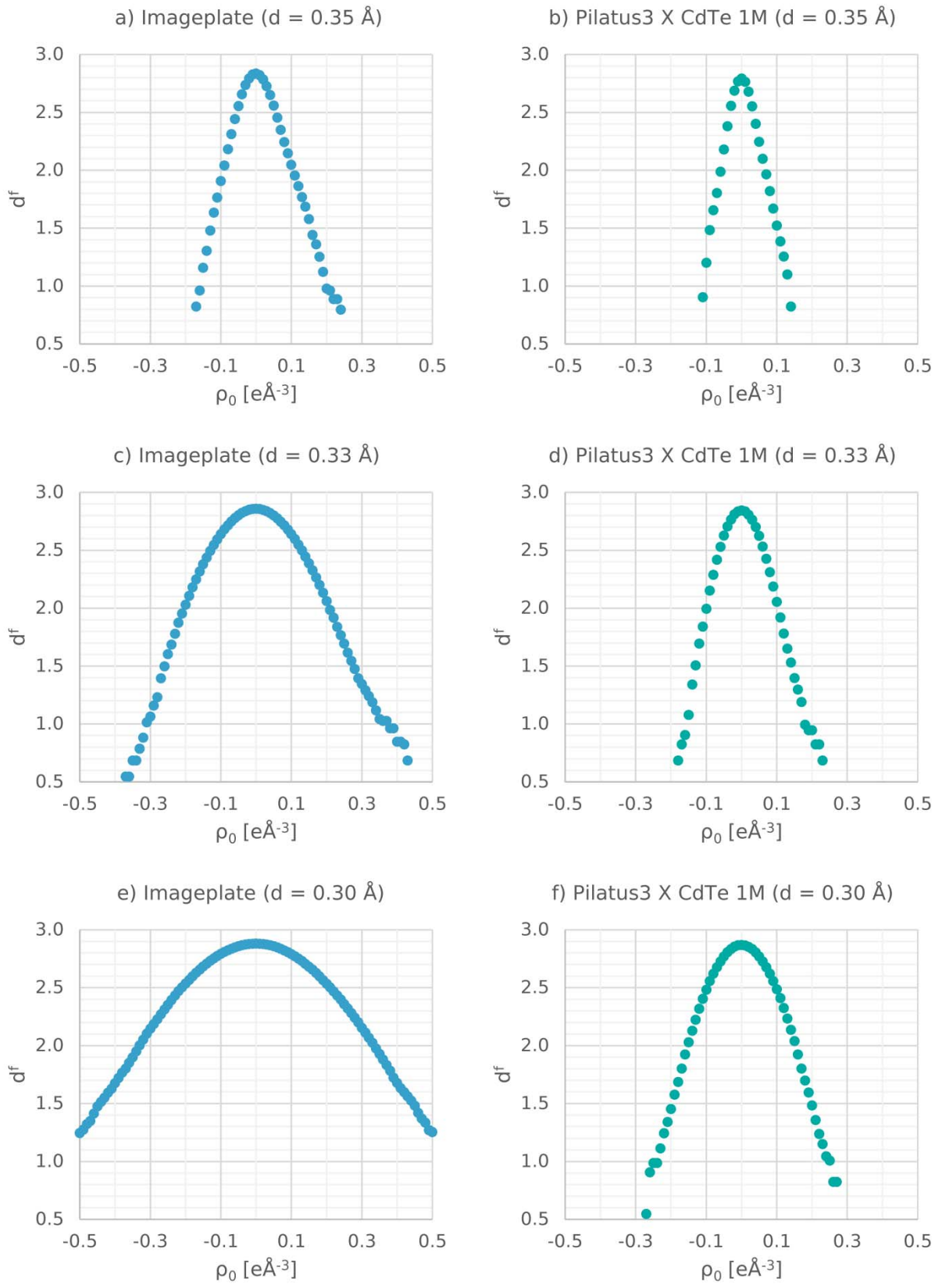

Figure S20 Fractal dimension plot for models derived from image plate and Pilatus3 data

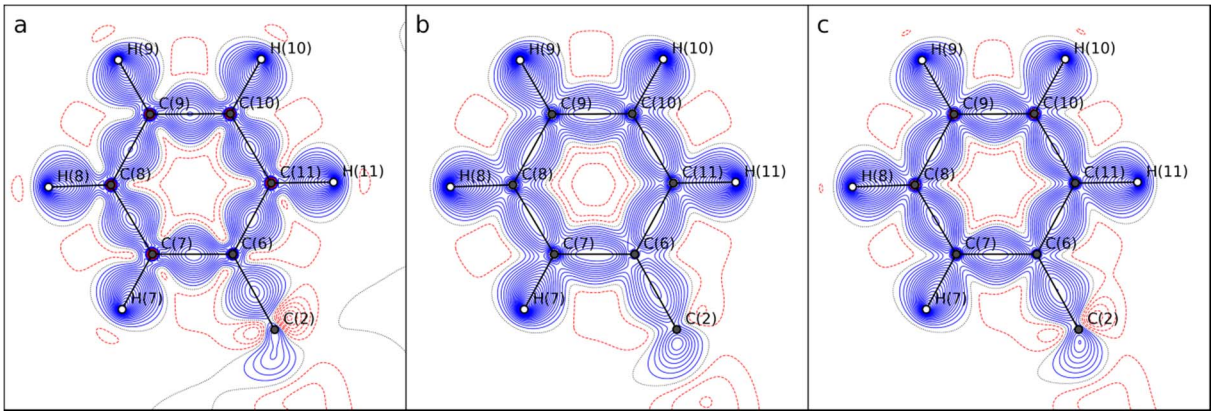

Figure S21 Deformation density (contour level of 0.05 eÅ^{-3}) for models derived from uncut experimental IP data (a), multipole projected theoretical density (b), uncut experimental P3 data (c). The term uncut refers to the following conditions: $I/\sigma(I)$ cut-off of -3, I cut-off of -3 and resolution of 1.67 Å^{-1}.

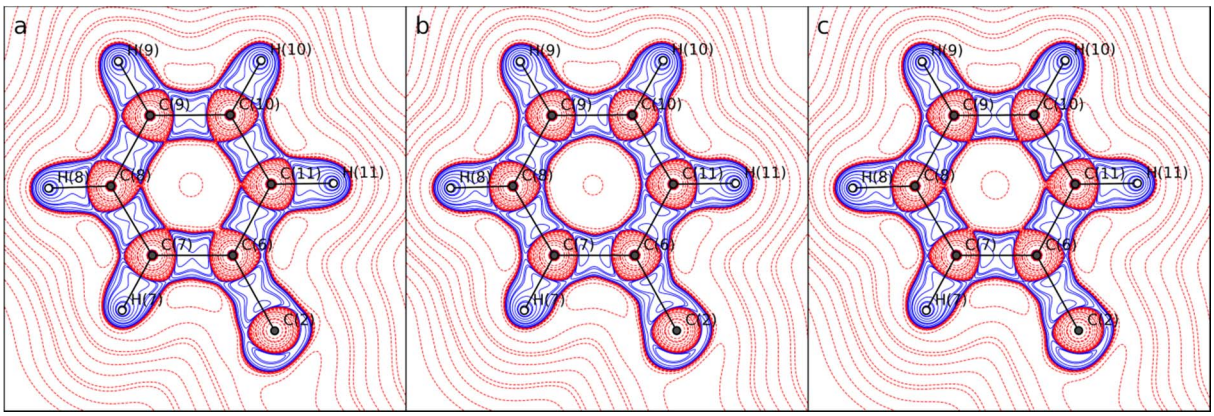

Figure S22 Laplacian (the contour levels are: $\pm$ a · 10^{b} eÅ^{-5}, with a = [1, 2, 4, 8], b = [-2, -1, 0, 1, 2, 3, 4]) for models derived from restricted experimental IP data (a), multipole projected theoretical density (b), restricted experimental P3 data (c). The term restricted refers to the following conditions: $I/\sigma(I)$ cut-off of 3 and resolution of 1.43 Å^{-1}.

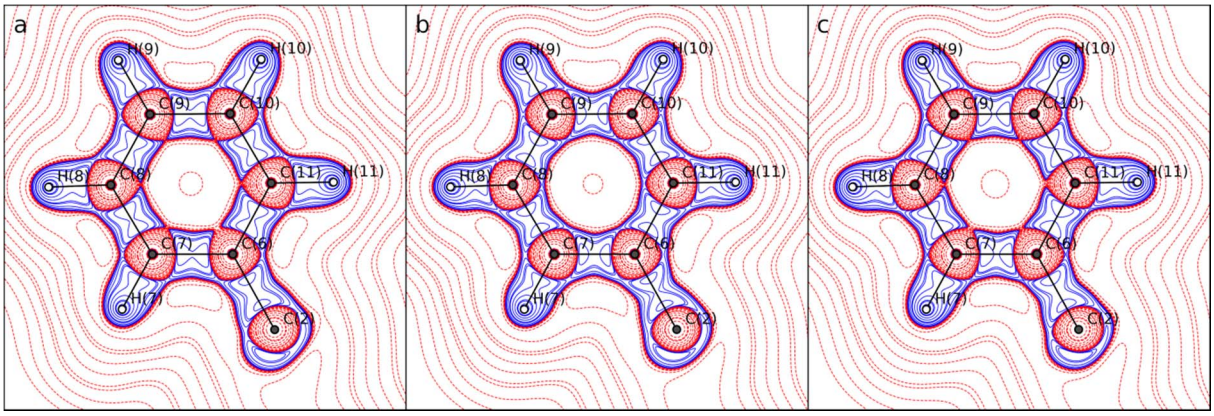

Figure S23 Laplacian (the contour levels are: $\pm$ a $\cdot$ 10^{b} eÅ^{-5}, with a = [1, 2, 4, 8], b = [-2, -1, 0, 1, 2, 3, 4]) for models derived from uncut experimental IP data (a), multipole projected theoretical density (b), uncut experimental P3 data (c). The term uncut refers to the following conditions: $I/\sigma(I)$ cut-off of -3, I cut-off of -3 and resolution of 1.67 Å^{-1}.

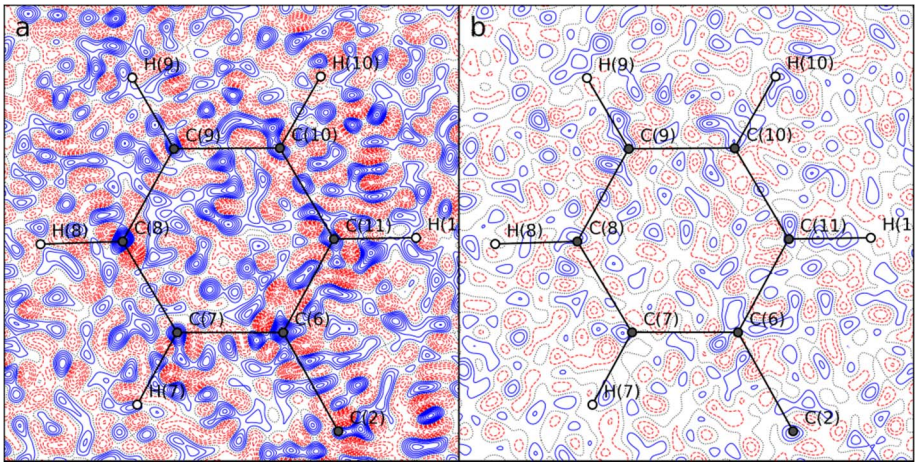

Figure S24 Residual density contour map (contour level of 0.05 eÅ^{-3}) for models derived from uncut experimental IP data (a) and uncut experimental P3 data (b). The term uncut refers to the following conditions: $I/\sigma(I)$ cut-off of -3, I cut-off of -3 and resolution of 1.67 Å^{-1}.